Celest Mech Dyn Astr (2009) 105:379–395
DOI 10.1007/s10569-009-9241-2

ORIGINAL ARTICLE

Orbital structure of self-consistent cuspy triaxial stellar systems

J. C. Muzzio · H. D. Navone · A. F. Zorzi

Received: 17 July 2009 / Revised: 18 September 2009 / Accepted: 19 October 2009 /
Published online: 31 October 2009

Abstract We used a multipolar code to create, through dissipationless collapses of systems of 10^6 particles, two cuspy self-consistent triaxial stellar systems with $\gamma \approx 1$. One of the systems has an axial ratio similar to that of an E4 galaxy and it is only mildly triaxial ($T = 0.914$), while the other one is strongly triaxial ($T = 0.593$) and its axial ratio lies in between those of Hubble types E5 and E6. Both models rotate although their total angular momenta are zero, i.e., they exhibit figure rotation. The angular velocity is very small for the less triaxial model and, while it is larger for the more triaxial one, it is still comparable to that found by Muzzio (Celest Mech Dynam Astron 96(2):85–97, 2006) to affect only slightly the dynamics of a similar model. Except for minor evolution, probably caused by unavoidable relaxation effects of the N-body code, the systems are highly stable. The potential of each system was subsequently approximated with interpolating formulae yielding smooth potentials, stationary in frames that rotate with the models. The Lyapunov exponents could then be computed for randomly selected samples of the bodies that make up the two systems, allowing the recognition of regular and of partially and fully chaotic orbits. Finally, the regular orbits were Fourier analyzed and classified using their locations on the frequency map. Most of the orbits are chaotic, and by a wide margin: less than 30% of the orbits are regular in our most triaxial model. Regular orbits are dominated by tubes, long axis ones in the less

J. C. Muzzio (✉)
Facultad de Ciencias Astronómicas y Geofísicas, Instituto de Astrofísica de La Plata (CONICET La Plata–UNLP), Universidad Nacional de La Plata, La Plata, Argentina
e-mail: jcmuzzio@fcaglp.unlp.edu.ar

H. D. Navone · A. F. Zorzi
Instituto de Física de Rosario (CONICET-UNR), Observatorio Astronómico Municipal de Rosario and Facultad de Ciencias Exactas, Ingeniería y Agrimensura de la Universidad Nacional de Rosario, Rosario, Argentina

H. D. Navone
e-mail: hnavone@ifir-conicet.gov.ar

A. F. Zorzi
e-mail: zorzi@ifir-conicet.gov.ar

triaxial model and short axis tubes in the more triaxial one. Most of the boxes are resonant (i.e., they are boxlets), as could be expected from cuspy systems.

Keywords Cuspy triaxial stellar systems · Figure rotation · Stellar orbits · Chaotic motion · Self-consistent models

1 Introduction

Self-consistent triaxial stellar systems, used to model elliptical galaxies, are much more difficult to build up than spherical or disk-like systems, many of which can be easily obtained through analytical or simple numerical methods (se, e.g., Binney and Tremaine 2008). The most popular method to obtain triaxial models is probably the one due to Schwarzschild (1979) which begins by assuming a certain density distribution, then computes a library of orbits in the potential generated by that distribution and, finally, determines the fractions of those orbits that are necessary to recover the proposed density distribution. Thus, one obtains not only the self-consistent system as the end product of this process but, in addition, an important by-product as is the orbital structure of that system as well.

It is not difficult to obtain a self-consistent system of N-bodies choosing an initial distribution of the bodies in the configuration and velocity spaces and following their evolution with an N-body code until an equilibrium is reached. Triaxial systems, in particular, can be obtained in different ways: deforming an initially spherical system (Holley-Bockelmann et al. 2001), following the collapse of a cold spherical system (Voglis et al. 2002; Muzzio et al. 2005), through mergers (Jesseit et al. 2005), and so on. Such systems would be of little use, however, if they remained as a mere collection of N-bodies whose positions and velocities were kept as computer files. Besides, while the motion of a star in a galaxy can be assimilated to the motion in a fixed and smooth potential, the potential of the N-body system is neither constant (due to statistical changes in the space distribution) nor smooth (because it is the sum of a large, but finite, number of potentials of individual bodies). The solution, pioneered by Sparke and Sellwood (1987), is to fit the N-body potential with an adequate mathematical expression which is then adopted as the fixed and smooth potential of the system. The orbital structure of the system can be subsequently obtained taking the positions and velocities of a sample of the N-bodies as initial conditions to compute orbits in that potential. This method which, for brevity, we will dub the N-body method is becoming increasingly popular and, in addition to the work cited above, we may also mention the recent investigations of Kalapotharakos and Voglis (2005), Aquilano et al. (2007) and Kalapotharakos (2008).

In other words, the end result of both methods is the same, i.e., a self-consistent stellar system whose orbital structure is known, but the path towards that result is different. Schwarzschild's method begins with the study of orbits in the potential of a certain density distribution and uses the knowledge obtained to build up the self-consistent system. The N-body method obtains a self-consistent system from the start and then investigates its orbital structure.

Nevertheless, it should be emphasized that getting a self-consistent system, by any method, does not guarantee that such system is stable in the long run, and much work has been devoted to the investigation of the stability of the models obtained by both methods. Since it is crucial for Schwarzschild's method to assign adequate weights at the regions of space visited by the different orbits, it has been notoriously difficult to construct truly stable models that harbor large fractions of chaotic orbits (see, e.g. Schwarzschild 1993; Merritt and Fridman 1996), despite the importance of chaos in stellar systems (Contopoulos 2002). Moreover, the

usual assumption that the density distribution has constant axial ratios throughout may also prevent the inclusion of significant fractions of chaotic orbits (Muzzio et al. 2005). Alternatively, highly stable models with large fractions of chaotic orbits are routinely built up with the N-body method (e.g., almost two thirds of the orbits in models E5 and E6 of Aquilano et al. 2007 are chaotic).

Thus, it seems advisable to increase the number of models built up and studied with the N-body method and that was one of the motivations of our previous work (Aquilano et al. 2007). Cuspy triaxial systems are a particularly interesting target because, on the one hand, they may offer the best models for elliptical galaxies and, on the other hand, they may include high fractions of chaotic orbits and are particularly difficult to build up with Schwarzschild's method (e.g. Merritt and Fridman 1996). In fact, using the N-body method, Holley-Bockelmann et al. (2001) were able to build several mildly triaxial models with $\gamma \approx 1$ in their central regions (where $\rho \propto r^{-\gamma}$, ρ being the density and r the radius) that were perfectly stable; moreover, Holley-Bockelmann et al. (2002) were able to grow black holes at the center of those models without affecting the triaxiality outside the innermost regions of the models. Curiously, however, those models had very few chaotic orbits.

An interesting result from the N-body method is that the triaxial models that it yields tend to exhibit figure rotation, that is, they rotate even though their total angular momentum is zero (Muzzio 2006; Aquilano et al. 2007). Angular velocities tend to be very low, corresponding to only one revolution in several Hubble times or, to put it differently, to corrotation radii that lie well outside the main body of the models. Thus, as could be expected, the dynamical consequences of this very slow rotation are minimal and the fractions of the different types of regular orbits are essentially the same, whether the system is rotating or not. Alternatively, there is a very small, but significant, increase in the fraction of chaotic orbits when the system rotates, probably due to the symmetry break caused by the rotation, and this increase can be attributed to the effect of the Coriolis force (see Muzzio 2006 for details). Nevertheless, to be coherent and to study precisely the same models yielded by the N-body method, the rotation was taken into account in the investigation of Aquilano et al. (2007) and we will do the same here.

The present investigation presents two cuspy ($\gamma \approx 1$) models built up using the same tools as in our previous papers (Muzzio et al. 2005; Aquilano et al. 2007). We plan to continue investigating cuspy triaxial stellar systems using the N-body code of Hernquist and Ostriker (1992), which is particularly adequate to investigate cuspy systems with $\gamma = 1$, so that the present work will offer an adequate bridge between our previous and future investigations.

The next section describes our models, Sect. 3 summarizes the methods used to investigate their orbital structure, Sect. 4 presents our results, and these are discussed in Sect. 5.

2 Stellar models

2.1 Triaxial stellar systems

Our previous models (Muzzio et al. 2005; Aquilano et al. 2007) were created following the recipe of Aguilar and Merritt (1990): randomly generate a spherical distribution of particles with a density inversely proportional to the distance to the center and a Gaussian distribution of velocities, and let it collapse following the evolution with a multipolar code until virial equilibrium is reached. In this way, one gets a triaxial system whose triaxiality depends on the value of the initial velocity dispersion, with lower dispersions yielding more triaxial systems, but the construction of cuspy models with this method proved to be challenging. It was clear from the start that we had to use low values of the softening parameter to avoid

that the density distribution flattened as we approached the center of the system, but values lower than about 0.0050 ruined the energy conservation of our integrations. Besides, we were unable to get more concentrated systems simply changing the radial distribution of bodies in the sphere that was allowed to collapse. Finally, using the same initial kinetic energy as we had used for our previous E6 model, we could obtain a reasonably cuspy triaxial system with the following method. We started with a spherical distribution of 10^6 particles (radius, mass and the gravitational constant were all set to unity), with a density inversely proportional to the distance to the center and Gaussian velocity distribution with the same velocity dispersion as that of the E6 model. The softening parameter was taken as $\epsilon = 0.0001$ and, as could be expected, although the collapse was followed for just 6.0 time units, energy was conserved only within 3%. As in our previous work, unbound particles were eliminated and the system was rotated to make coincide the major, intermediate and minor axes of inertia with the x, y and z axes, respectively. Thereafter, we computed the potential energy of every particle, first with a softening parameter of $\epsilon = 0.0050$ and then without that parameter, and the differences between both results were obtained. A Schuster (or Plummer) law was then used to fit the relationship between those differences and the distance to the center of the corresponding particles. For the subsequent evolution, the softening parameter was taken as $\epsilon = 0.0050$ and the Schuster potential was added to that of the N-bodies. In other words, as the softening makes the potential of the N-bodies different from the one that would have been obtained without softening (i.e., with Newtonian particles), we compensate for that difference adding the Schuster potential. The change in the total potential energy was 1.6% only, but the addition was very effective to preserve the cuspy density distribution obtained from the initial collapse and, moreover, the resulting potential is essentially the one due to a distribution of Newtonian (not softened) particles. The system was evolved for 300 crossing times (T_{cr} hereafter), the 2% less tightly bounded particles that had not reached equilibrium were eliminated and the inertia axes rotated again to coincide with the coordinate axes. The differences between the potentials with and without softening were recomputed, a new Schuster potential was fitted to them and the system was evolved for another 100 T_{cr} to obtain the model finally adopted. An additional $1,000$ T_{cr} run was used to check for stability and to obtain the angular velocity of figure rotation and we dubbed this model E6c. Despite the long integration times, energy was conserved within 3×10^{-3} during the 300 T_{cr} integration and within 1×10^{-2} during the $1,000$ T_{cr} integration. The N-body code insures that the total angular momentum is essentially zero at all times (see Muzzio 2006 for details).

Nevertheless, it was impossible to get less flattened cuspy models with the same method. We reasoned that, as more initial kinetic energy was needed, the larger velocity dispersion near the center of the systems was ruining the cuspy density distribution. Therefore, instead of taking a constant velocity dispersion for the initial distribution of particles, we took a velocity dispersion that was essentially zero (actually, 0.0001) at the center and rised linearly toward the border; in this case the total initial kinetic energy was made equal to that of the E4 system of Aquilano et al. (2007). Except for that different way of choosing the initial velocity dispersion, all the other steps were the same followed to obtain the model E6c. This time we succeded and we obtained the cuspy model referred to as E4c hereafter.

Table 1 lists, for each model, its final mass, crossing time, effective radius, central radial velocity dispersion and angular velocity of figure rotation. The effective radius was computed for the (x, z) projection and, correspondingly, the central radial velocity was computed from the y velocities of the 10,000 particles closer to the center on that projection.

Our models are scale free but one can get some idea of what our units mean through a comparison with real galaxies. Following Aquilano et al. (2007), we have chosen galaxies NGC1379 and NGC4697 (Napolitano et al. 2005; Forbes and Ponman 1999), whose

Table 1 Properties of our models

Model	Mass	T_{cr}	R_e	σ_o	ω
$E4c$	0.905	0.490	0.195	0.870	0.00037 ± 0.00006
$E6c$	0.803	0.278	0.110	0.969	0.01258 ± 0.00037

Table 2 Major semiaxis and semiaxial ratios of our models

Model	Prop	20 (%)	40 (%)	60 (%)	80 (%)	100 (%)
$E4c$	a	0.068	0.112	0.161	0.243	0.537
	b/a	0.550	0.553	0.589	0.646	0.735
	c/a	0.453	0.473	0.528	0.602	0.707
$E6c$	a	0.046	0.079	0.107	0.148	0.330
	b/a	0.663	0.668	0.718	0.729	0.745
	c/a	0.487	0.433	0.452	0.458	0.436

mass-to-light ratio gradients are zero. Comparing the observed values for those galaxies with those of our Table 1 suggests that values between about 13 kpc and 52 kpc can be used as length unit and values between about 0.09 Gy and 0.28 Gy as time unit. Therefore, the Hubble time can be estimated as between 50 and 150, and we adopt a value of 100 in what follows. It may be noticed that this value is much shorter than the intervals used to create our models, but we are only interested in getting truly stable systems for our study of their orbital structure and not in creating them through a realistic process.

We computed the major semiaxis (a) and the ratios of the intermediate (b) and minor (c) semiaxes to the major one for the 20%, 40%, ... and 100% most tightly bound particles for our models and the results are given in Table 2. For both models the axial ratios change with the distance to the center, and we adopt the values corresponding to the 80% most bounded particles to characterize them. We notice that the c/a ratio is similar to that of an E4 galaxy for the E4c model, and intermediate between those of E5 and E6 galaxies for the E6c model; nevertheless, as the E6c model was create using the same initial energy we had used to create our previous E6 model (Aquilano et al. 2007), we preferred to dub it E6c, rather than E5.5c. It is just fair to say that the identification of our models with elliptical galaxies of a given Hubble type refers to their geometry only and that there is no guarantee that the dynamics of our models are the same as those of true galaxies. We just want to see whether it is possible to have strongly triaxial and cuspy models, that might represent elliptical galaxies, and that are highly stable despite containing high fractions of chaotic orbits.

A comparison of the present Table 2 with that of Aquilano et al. (2007) is interesting. The triaxiality ($T = (a^2 - b^2)/(a^2 - c^2)$) values of models E4, E5 and E6 were, respectively, 0.985, 0.814 and 0.778, while those of models E4c and E6c are, respectively, 0.914 and 0.593, that is, the new models are substantially *more* triaxial than the equivalent previous ones. Other differences are also apparent: (1) The a values for the different fractions of most tightly bound orbits show that the new models are more concentrated than the equivalent previous ones; (2) Model E4 was almost perfectly rotationally symmetric, while model E4c clearly departs from rotational symmetry; (3) Although the c/a value of the 80% most tightly bound particles of model E6c falls in between the corresponding values of models E5 and E6, most of the other b/a and c/a values of model E6c are higher than those of models E5 and E6. In other words, and not surprisingly, the density distributions of the present models are appreciably different than those of the equivalent previous ones, a fact that should be kept in mind when comparing the results of both investigations.

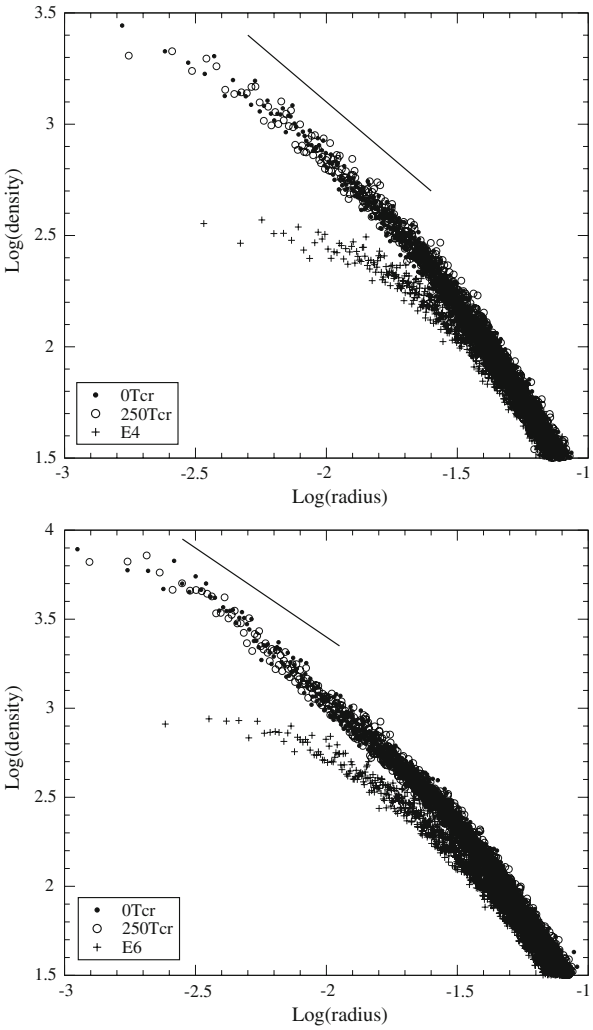

Fig. 1 Log–log plot of density versus radius for the central parts of model E4c (*above*) and E6c (*below*). Different symbols are used to show the profiles at two different times. The corresponding plots for the E4 and E6 models of Aquilano et al. are also shown for comparison. The full lines correspond to slopes $\gamma = 1.0$

Figure 1 gives log–log plots of density versus radius for the central parts of both models. The densities were computed in a sphere (for the smallest radius) and in spherical shells (for the other radii) containing 100 particles each, so that the relative Poissonian error of each point in the plot is about 0.043. Long term evolution of the models will be discussed below, but we have used here different symbols to represent profiles separated by 250 T_{cr} and no significant evolution is evident from the plots. We notice that the present models are indeed much more cuspy than the previous ones, also plotted for comparison: the central density is now an order of magnitude larger and the present profiles have central slopes close to $\gamma = 1$ before leveling off at radii about $1/4$ or $1/3$ shorter than in our previous models.

2.2 Smooth stationary potential

Since the N-body potentials are neither smooth nor stationary, in order to be able to compute orbits and Lyapunov exponents we represented them with the same quadripolar

approximation used in our previous work (an equivalent expression was used by Schwarzschild 1979):

$$\Phi(\mathbf{r}) = f_{00}(p_1) + f_{xx}(p_2)x^2 + f_{yy}(p_2)y^2 + f_{zz}(p_2)z^2, \tag{1}$$

where:

$$f_{yy}(p_2) = -f_{xx}(p_2) - f_{zz}(p_2), \tag{2}$$

and where p_i are the softened radii, given by:

$$p_1^2 = r^2 + \epsilon^2, \tag{3}$$

for the monopole and by:

$$p_2^2 = r^2 + 2\epsilon^2, \tag{4}$$

for the higher order terms (see White 1983 for details). The f values were computed from the N-body distribution and fitted with equations of the form:

$$f(p_i) = C \exp\left(\sum_{n=1}^{4} a_n [\ln(p_i + e)]^n\right). \tag{5}$$

To this potential, computed with $\epsilon = 0.0050$, we added the Schuster (or Plummer) potentials we had used to compensate for the softening. They are:

$$\Phi(r) = -0.00189/(r^2 + 0.00582^2), \tag{6}$$

for the $E4c$ model and:

$$\Phi(r) = -0.00280/(r^2 + 0.00459^2), \tag{7}$$

for the $E6c$ model.

In both cases the square root of the mean square percentual difference between the N-body and the smoothed potential was close to 0.4%, i.e., similar to the accuracy obtained by Muzzio et al. (2005), Carpintero and Wachlin (2006), Muzzio (2006) and Aquilano et al. (2007).

Since the rotation velocities are significant according to their computed errors, we have taken them into account and the above potentials were placed in adequate rotating systems. The corresponding Hamiltonian and equations of motion can be found, e.g., in Binney and Tremaine (2008) where we can also see that the centrifugal force terms are $\omega^2 x$ and $\omega^2 y$, while the Coriolis force ones are $-2\omega v$ and $2\omega u$ (where u and v are the velocity components along the x and y axes, respectively). The sizes and internal velocities of the present models are of the same order of magnitude as those of the one studied by Muzzio (2006), as is the rotational velocity of model E6c, while that of model E4c is much lower. Therefore, the dynamical consequences of rotation on our model E6c are probably as small as those on the model of Muzzio (2006) and negligibly small on our model E4c. Since in the former model the average velocities of the bodies are of the order of unity, the average distances an order of magnitude lower than that, and ω^2 two orders of magnitude smaller than ω it is clear that, as concluded by Muzzio (2006), most of the dynamical effects of rotation should be due to the Coriolis, rather than to the centrifugal, forces.

2.3 Long term evolution

In order to check for possible long term evolution and to derive the angular velocity of rotation, the models were let to evolve for $1,000 T_{cr}$ as indicated above. As in our previous studies (Muzzio 2006; Aquilano et al. 2007), the plots of the angle of the major axis with respect to its initial direction against the time were slightly curved, probably as a result of gradual evolution (see below). Therefore, since the models we are using are the initial ones of this final run, we fitted parabolae to the data and took their tangents at the origin as the angular velocities, just as we had done in our previous work.

The long term evolution was investigated through the changes suffered by the semiaxes and the central density (computed from the 10,000 particles closer to the center) of both systems. Those changes ranged between 0.9% and 4.1% over a Hubble time, and are most likely caused by the relaxation effects of the multipolar code (see, e.g. Hernquist and Barnes 1990). Two additional series of experiments were run to check that hypothesis. First, we integrated all the bodies of each model in the corresponding fixed and softened potential (thus eliminating the relaxation effects) and in this case the changes were generally smaller and below the corresponding statistical errors. Second, we run another full N-body integration using only one-tenth of the original particles and increasing their masses ten fold (thus increasing the relaxation effects) and, in this case, the changes were substantially larger ranging between 1.6% and 7.9%. We may thus conclude that our models are highly stable over intervals of the order of a Hubble time and that the small changes observed are due to relaxation effects of the N-body code.

The good fitting of the interpolated potential as the models evolve was extensively checked by Muzzio et al. (2005) and Carpintero and Wachlin (2006). Besides, Muzzio (2006) showed that fitting the potential to the N-body distribution at different times yielded negligibly small differences in the percentages of chaotic and regular orbits; similar conclusions had been reached by Voglis et al. (2002) with a different N-body code.

3 Orbital analysis

3.1 Lyapunov exponents

The six finite time Lyapunov characteristic numbers (FT-LCNs hereafter) were computed using the LIAMAG routine (Udry and Pfenniger 1988), kindly provided by D. Pfenniger, as in our previous investigations. We selected at random 3,622 and 4,013 of the bodies that make up, respectively, the systems E4c and E6c, and we used their positions and velocities as initial positions and velocities to compute orbits and FT-LCNs in the corresponding stationary smooth potentials rotating with the angular velocities found for each system. As before, the integration and normalization intervals were taken, respectively, as 10,000 and 1, the requested precision as 10^{-15} and energy was generally conserved to better than 10^{-12}. Volume conservation in phase space demands that the six Lyapunov exponents appear in pairs of the same absolute value and opposite sign, while due to energy conservation one of those pairs has zero value. As a result, there are only two independent FT-LCNs, the largest of which will be referred to as L_{max} and the second largest one as L_{int} hereafter.

The use of a finite integration interval to obtain the FT-LCNs, rather than the infinite one used to define the Lyapunov exponents, results in a limiting minimum value, L_{lim}, larger than zero (see Sect. 4.1 below). Thus, as in our previous works, we classify orbits as regular if $L_{max} < L_{lim}$, as partially chaotic if $L_{int} < L_{lim} \leq L_{max}$ and as fully chaotic if $L_{lim} \leq L_{int}$.

3.2 Frequency analysis and regular orbit classification

The modified Fourier transform code of Šidlichovský and Nesvorný (1997), kindly provided by D. Nesvorný, was used for the frequency analysis of the regular orbits, as we had done in Muzzio (2006) and Aquilano et al. (2007). The same initial positions and velocities selected to obtain the FT-LCNs were used, and the frequency analyses to obtain the fundamental frequencies F_x, F_y and F_z were performed, respectively, on the complex variables $x+iu$, $y+iv$ and $z+iw$; these were derived from 8,192 points equally spaced in time obtained integrating the regular orbits over 300 radial periods. In this way, as indicated by Muzzio (2006), frequencies can be obtained with a precision better than 10^{-9} for isolated lines; nevertheless, the precision is much lower when there are nearby lines and the practical limit of 2×10^{-4} for the precision, adopted in that work and by Aquilano et al. (2007), is also used here.

Regular orbits were then classified as boxes and boxlets (BBLs hereafter), long axis tubes (LATs hereafter) or short axis tubes (SATs hereafter) using the method of Muzzio (2006) and taking into account the additional improvements introduced by Aquilano et al. (2007). The main difference with the original method of Kalapotharakos and Voglis (2005) is that one should not always take as the fundamental frequency the one corresponding to the maximum amplitude, as shown by Binney and Spergel (1982) and Muzzio (2006).

Our classification code failed to classify three orbits of model E4c and one orbit of model E6c. Visual inspection of the spectra of those orbits revealed that: (1) Those of model E4c seemed to be perfectly normal LATs that could have been classified by the code, had we used a value larger than 2×10^{-4} as the limit for the precision of the frequencies; (2) The orbit of model E6c was just an (x, z) banana (i.e., obeying the [2,0,−1] resonance) that had a mean z value larger than its amplitude, so that the frequency corresponding to the largest z amplitude was essentially zero. A more detailed investigation of the orbits of the E4c model that could not be classified, using FT-LCNs computed over 100,000 intervals and spectra obtained over different intervals, suggested that those three orbits might be weakly chaotic. Therefore, we decided not to alter the limit for the precision of the frequencies and we simply chose the proper fundamental frequencies from visual inspection of their spectra. Nevertheless, we did improve the code to allow it to find bananas whose mean value is larger than its amplitude, like the one of model $E6c$.

A score of the LATs of model E4c turned out to have $F_x/F_z < 0.5$ and they occupied anomalous positions in an energy versus F_x plot. We found that they all had the amplitude anomaly Muzzio (2006) had found for some SATs. We improved again our classification code, selecting the principal F_x frequency of the LATs with the same criterium used to select the principal F_z frequency of the SATs (i.e., we do not select the frequency with the largest amplitude but the frequency with the second largest amplitude when the latter frequency is larger than the former one and the amplitude of the latter is larger than 0.7 of the former). After that improvement, only one LAT still had $F_x/F_z < 0.5$, and it turned out that both its spectrum and the value of its FT-LCNs computed over an 100,000 interval suggested that it was mildly chaotic. Visual inspection of its spectrum did not suggest any possible improvement to the frequency values chosen by the program, so that we kept those values.

Two SATs of the E6c model have $F_x/F_z = F_y/F_z \simeq 0.54$ and are clearly separated from the other SATs of the same model which all have $F_x/F_z = F_y/F_z > 0.70$. Table 3 gives, for each of those two orbits, the spectra corresponding to each coordinate axis; only the six largest amplitude lines are given and the figures are limited to four decimals. The spectra resemble those of regular SATs, with many coincidences between the frequencies of x and y lines; moreover, there is no suggestion of chaoticity in these spectra. Nevertheless, the (x, y) and (x, z) projections of those orbits, shown in Fig. 2, reveal that they are definitely

Table 3 Results of the frequency analysis of orbits 2399 and 3209 of model E6c

Orbit	F_x	F_y	F_z	A_x	A_y	A_z
2399	−0.4365	−0.4365	−0.0380	1.5834	0.0241	0.2129
	0.4365	−1.3096	0.0380	0.6209	0.0129	0.1975
	−1.3096	0.4365	−0.8350	0.3276	0.0095	0.1317
	−2.1827	−2.1827	−1.7081	0.1775	0.0094	0.0651
	−3.0557	−0.1254	−0.9111	0.1220	0.0089	0.0544
	−3.9288	−3.0557	−2.5811	0.0931	0.0074	0.0451
3209	−0.2811	−0.2811	−0.0517	1.8072	0.0424	0.4713
	0.2811	−0.0742	0.0517	1.0140	0.0293	0.4248
	−0.8433	0.0742	−0.5105	0.3362	0.0252	0.2968
	−1.4054	0.2811	−1.0726	0.1737	0.0238	0.1285
	−1.9676	−0.0943	0.5105	0.1163	0.0212	0.0961
	−2.5298	−0.8433	−1.6348	0.0874	0.0201	0.0840

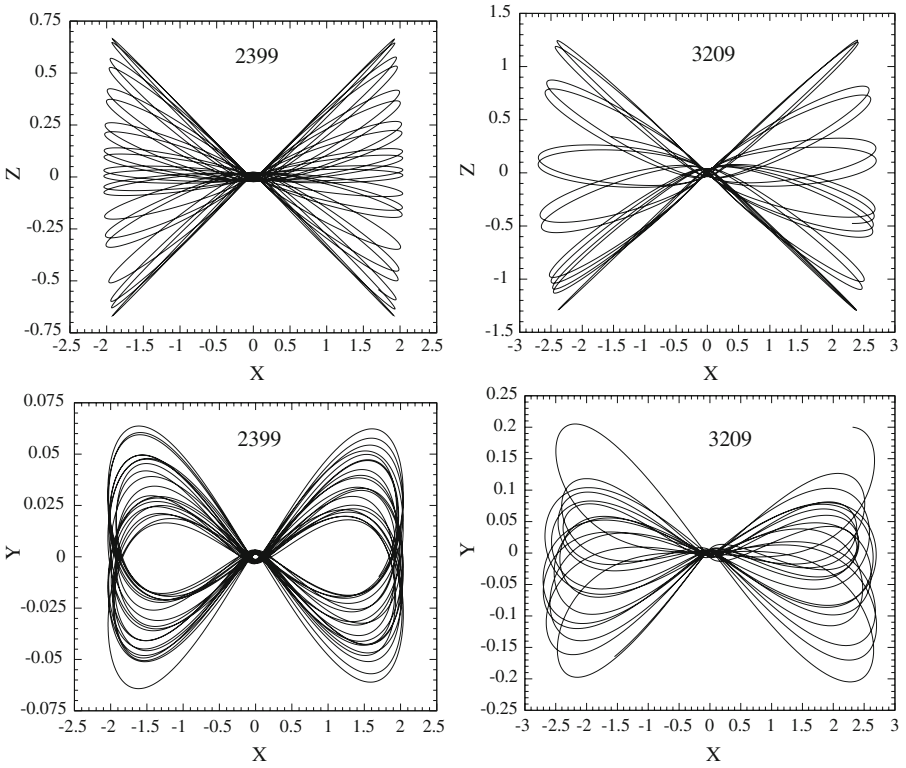

Fig. 2 Orbits 2399 (*left*) and 3209 (*right*) of the E6c model. Note the very different scales, as the orbits are strongly concentrated towards the (x, z) plane

not SATs, but boxlets. Clearly, these two orbits cannot be classified from their spectra alone. Thus, we resorted to the use of the energy versus frequency plane, whose usefulness has been stressed by Muzzio (2009) and, comparing the frequencies of those orbits with the fundamental frequencies of other orbits of the same energy, we decided to adopt $F_x = 0.4365338$, $F_y = 1.3095981$ and $F_z = 0.8350364$ as the fundamental frequencies of orbit 2399 and $F_x = 0.2810892$, $F_y = 0.487959595$ and $F_x = 0.5104582$ as those of orbit 3209. The former corresponds to a (3,−1,0) resonance and the latter to a (9,−1,−4) resonance (see Sect. 4.2), i.e., they are boxlets. It is clear from Fig. 2 that orbit 2399 obeys the (3,−1,0) resonance, but the character of orbit 3209 is much more contrived and it is not obvious from that figure; nevertheless, we extended the integration of that orbit to 10,000, and the plots revealed that it always keeps out from a small central region, confirming its boxlet character.

A more refined classification was performed later, separating the inner from the outer LATs, using the energy versus F_x/F_z plane as explained by Aquilano et al. (2007), and selecting the most important resonances in order to separate the boxlets according to the resonances that they obey, as we explain in Sect. 4.2.

4 Results

4.1 Chaotic orbits

As in our previous work, the FT-LCNs were obtained from numerical integrations over a finite interval, $T = 10{,}000$, rather than the infinite one required to obtain the Lyapunov exponents. Therefore, their values are not zero for regular orbits but there is a limiting value, $L_{lim} \approx lnT/T \approx 0.00092$, that should be regarded as their zero value. Inspection of plots of the FT-LCNs versus the energy of the orbit and of L_{max} versus L_{int} showed that the limiting value should be taken as $L_{lim} = 0.00180$, rather than as 0.00155 as in our previous work; the present limiting value corresponds to a Lyapunov time of 556, i.e., five times longer than the Hubble time.

Aquilano et al. (2007) extensively discussed why to use such small limiting values for the Lyapunov exponents, rather than 0.0100, which would correspond to a Lyapunov time comparable to the Hubble time. The reason is that the Lyapunov time gives the scale for the exponential divergence of orbits, but here we are interested on the relationship between the space distribution of orbits and the values of their Lyapunov coefficients. Besides, just as it happened in our previous paper, quite a few orbits with $0.0018 < L_{max} < 0.0100$ (26 of model E4c and 1 of model E6c) could not be classified by our frequency analysis code and examination of their spectra showed lines of similar frequencies and amplitudes, typical of chaotic orbits. That is, despite their low L_{max} values, those orbits reveal their chaotic nature.

As in our previous paper, we separated the orbits of each model in three groups: (1) Those with $L_{max} < 0.0018$, that is, those that are classified as regular with both choices of L_{lim} (REGREG hereafter); (2) Those with $0.0018 \leq L_{max} < 0.0100$, that is, those that are classified as regular with $L_{lim} = 0.0100$ but as chaotic with $L_{lim} = 0.0018$ (REGCHAO hereafter); (3) Those with $0.0100 \leq L_{max}$, that is, those that are classified as chaotic with both choices of L_{lim} (CHAOCHAO hereafter). We then took, for each orbit, 11 (x, y, z) values separated by intervals of 10, that is, over a total interval of about one Hubble time, and we computed the mean square value of each coordinate; Table 4 gives the square roots of the ratios of the y and z mean square values to the x mean square value for each model and for each group. The results for both models show that the axial ratios of the REGCHAO orbits are lower than those of the CHAOCHAO orbits, as could be expected from the results of Muzzio

Table 4 Axial ratios of the different classes of orbits for different choices of L_{lim}

Ratio	System	REGREG (%)	REGCHAO (%)	CHAOCHAO (%)
y/x	E4c	0.757 ± 0.018	0.696 ± 0.023	0.826 ± 0.023
	E6c	0.863 ± 0.024	0.486 ± 0.040	0.755 ± 0.020
z/x	E4c	0.685 ± 0.019	0.684 ± 0.023	0.784 ± 0.022
	E6c	0.310 ± 0.026	0.342 ± 0.040	0.531 ± 0.018

Table 5 Percentages of regular and chaotic orbits in the triaxial systems

Mod	Regular (%)	Part. Ch. (%)	Fully Ch. (%)
E4c	34.46 ± 0.79	12.18 ± 0.54	53.37 ± 0.83
E6c	29.06 ± 0.72	6.53 ± 0.39	64.42 ± 0.76

Table 6 Axial ratios of the different classes of orbits in our models

Ratio	System	Regular (%)	Part. Ch. (%)	Fully Ch. (%)
y/x	E4c	0.757 ± 0.018	0.759 ± 0.024	0.726 ± 0.022
	E6c	0.863 ± 0.024	0.528 ± 0.048	0.706 ± 0.020
z/x	E4c	0.685 ± 0.019	0.705 ± 0.024	0.746 ± 0.021
	E6c	0.310 ± 0.026	0.334 ± 0.043	0.508 ± 0.019

and Mosquera (2004), Muzzio et al. (2005) and Aquilano et al. (2007) because the former have lower L_{max} values. Besides, although the results for the REGREG and REGCHAO are essentially the same for the E4c model and the z/x ratio of the E6c model, they differ significantly for the y/x ratio of the E6c model. Thus although not as clearly as it was the case with the models of Aquilano et al. (2007), we see that orbits with $0.0018 \leq L_{max} < 0.0100$ exhibit, over intervals comparable to a Hubble time, a spatial distribution that differs from that of regular orbits. Therefore, we adopted $L_{lim} = 0.0018$, equivalent to the 0.00155 value of all our previous works.

Table 5 gives the percentages of regular, partially and fully chaotic orbits in our models. As in our previous work, the statistical errors have been estimated from the binomial distribution.

For each model and for each class of orbits we used 11 (x, y, z) orbital positions taken at 10 intervals (i.e., over a total interval equivalent to a Hubble time) to make plots of the (x–y) and (x–z) projections of the orbits. These plots did not show as clearly as and Fig. 4 of Muzzio et al. (2005) and Fig. 3 of Aquilano et al. (2007) differences among the distributions of the different classes of orbits, a fact corroborated by Table 6 which gives, separately for each model and for each class of orbit, the axial ratios of the corresponding distributions, computed from the square roots of the mean square values of each coordinate. For the E4c model, the y/x axial ratios of the different classes of orbits are essentially the same and, although the z/x ratios show the usual trend (increasing from the regular orbits to the fully chaotic ones), that trend is not significant considering the errors involved. The z/x ratios of the E6c model clearly show that the distribution of the regular orbits is more flattened than that of the fully chaotic ones and, despite the large error of that ratio for the partially chaotic orbits, it is plain that it is lower than the corresponding one for the fully chaotic orbits. Finally, the behaviour of the y/x ratio of the E6c model is completely different from that in our previous models, which showed a general increase of that ratio when going from regular to fully chaotic orbits.

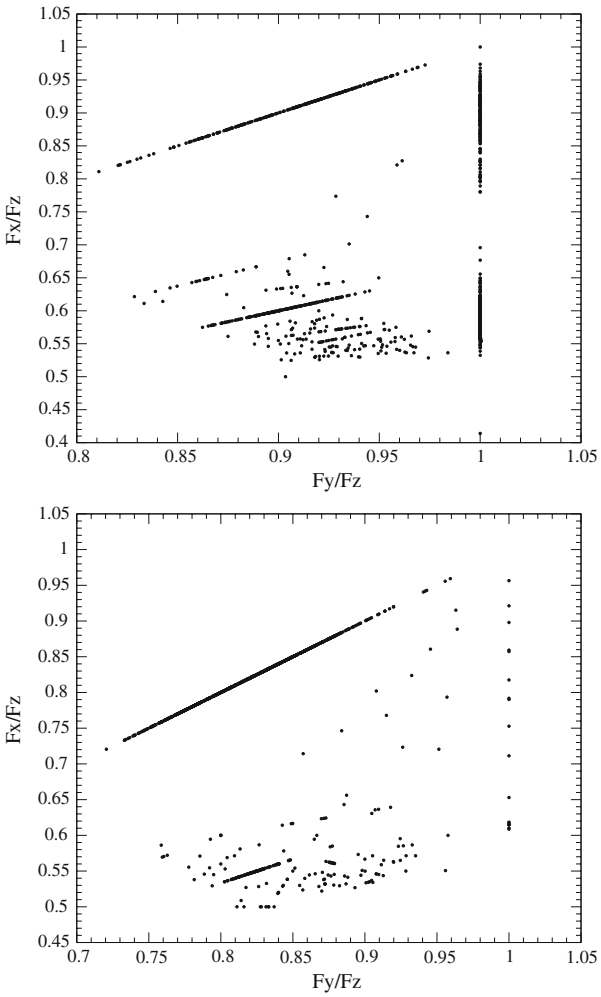

Fig. 3 Frequency maps for the E4c (*top*), and E6c (*bottom*) models

4.2 Regular orbits

Figure 3 presents the frequency maps of our models. The vertical distribution at $F_y/F_z = 1$ corresponds to the LATs, the diagonal at the upper left corresponds to the SATs, and the rest of the dots represents the BBLs with several resonances (boxlets) that stand out clearly from the maps. Notice, however, that as explained in Sect. 3.2 the low F_x/F_z value of the E4c LAT at $F_x/F_z = 0.414$ is probably due to that orbit being mildly chaotic. Also, the fundamental frequencies adopted for the peculiar orbit 2399 of model E6c place it outside the limits of the corresponding frequency map.

Several resonances can be visually identified on the frequency maps but, since their structure is more complicated than that of the maps of Aquilano et al. (2007), we preferred to make the computer to systematically search for all possible resonances:

$$l F_x + m F_y + n F_z = 0, \tag{8}$$

Table 7 Percentages of the different types of regular orbits

Type	E4c (%)	E6c (%)
Inner LAT	32.77 ± 1.33	1.46 ± 0.35
Outer LAT	14.58 ± 1.00	0.17 ± 0.12
SAT	21.96 ± 1.17	77.44 ± 1.22
Box (≤ 5)	5.93 ± 0.67	3.34 ± 0.53
(2,0,−1)	0.08 ± 0.08	0.51 ± 0.21
(2,1,−2)	0.64 ± 0.23	1.63 ± 0.37
(3,−2,0)	14.10 ± 0.99	9.01 ± 0.84
(3,−1,−1)	1.04 ± 0.29	0.86 ± 0.27
(3,−3,1)	0.40 ± 0.18	0.51 ± 0.21
(4,−3,0)	1.68 ± 0.36	0.34 ± 0.17
(5,−3,0)	1.60 ± 0.36	0.17 ± 0.12
(5,−2,−1)	1.84 ± 0.38	0.43 ± 0.19
Other (≤ 5)	1.36 ± 0.33	2.14 ± 0.42
Periodic	2.00 ± 0.40	1.97 ± 0.41

Table 8 Percentages of boxes as fraction of boxes plus boxlets

Order	E4 (%)	E5 (%)	E6 (%)	E4c (%)	E6c (%)
≤ 5	78.5 ± 2.1	64.3 ± 1.6	65.8 ± 1.7	19.5 ± 2.0	16.4 ± 2.4
≤ 10	43.7 ± 2.5	36.2 ± 1.6	36.5 ± 1.7	8.4 ± 1.4	7.6 ± 1.7

with l, m and n integers not all equal to zero. We limited our search to l, m and n absolute values smaller than, or equal to, 5 (i.e., the highest order resonances found in our previous work). The percentages of the different types of regular orbits in each model are given in Table 7; we give explicitly the results for all the resonances that were included in Aquilano et al. (2007) plus those of the (3,−1,−1) resonance that yields a little more than 1% of the regular orbits of model E4c, but all the other resonances which individually amounted to less than 1% of the regular orbits, were bunched together under $Other(\leq 5)$. Similarly, $Box(\leq 5)$ gives the percentages of all the orbits that were classified neither as SATs, nor as LATs, and for which no resonances were found up to order 5. Orbits obeying more than one resonance were classified as periodic. The errors were estimated from the binomial distribution.

To investigate further the relationship between cuspiness and boxlets, we also searched for resonances up to order 10 and we repeated these searches, up to orders 5 and 10, with our previous models. Table 8 gives the percentages of boxes (i.e., those orbits that are neither LATs nor SATs, and for which no resonance up to a certain order could be found, relative to those that are neither LATs nor SATs) for the different models and for the two limits to the order of resonance.

5 Discussion and conclusions

Aquilano et al. (2007) had already shown that it is perfectly possible to build self-consistent stellar models of elliptical galaxies that are highly stable in spite of containing high fractions of chaotic orbits. The present work strengthens that conclusion and extends it to even higher chaoticity levels (more than 70% of the orbits of model E6c are chaotic). Moreover, the present models are cuspy, with $\gamma \approx 1$, and at least model E6c is highly triaxial ($T = 0.593$).

Our success at building such stable models is most likely due to the fact that we did not use the method of Schwarzschild (1979), but we built our models from N-body collapses, as indicated by Muzzio et al. (2005). It is worth recalling that Holley-Bockelmann et al. (2001) also succeded in building stable cuspy triaxial models, albeit less triaxial than ours and with little chaos, using an N-body method.

As could be expected, the presence of the cusps enhances chaoticity. Not only the fractions of chaotic orbits in the present models are higher than those in the equivalent non-cuspy models of our previous work, but the FT-LNC values are now higher. The largest L_{max} values in our E4c and E6c models are, respectively, 1.717 and 2.391, while those of models E4 and E6 of Aquilano et al. (2007) are 0.261 and 0.572, respectively. The increase of chaoticity with triaxiality is also clear. All these results agree well with those of Kandrup and Sideris (2002) and Kandrup and Siopis (2003).

Regarding our regular orbits classification code it turned out that, with only a handful of exceptions, several of which can be easily explained as being due to mildly chaotic orbits, our code can now classify virtually all the orbits of the models of Muzzio (2006), Aquilano et al. (2007) and the present ones, which comprise a grand total of 20,575 orbits. In fact, only orbits 2399 and 3209 of model E6c seem to be impossible to classify from their spectra alone (we had to add energy information to be able to classify them from their spectra), which gives a failure rate of less than 1 over 10,000. Alternatively, the method of Carpintero and Aguilar (1998) leaves between 10% and 15% of unclassified orbits (see Muzzio et al. 2005; Jesseit et al. 2005). Nevertheless, as pointed out by Muzzio (2009), it is clear that our code has demanded successive improvements as we explored different models (i.e., almost rotationally symmetric, cuspy, and so on) and in all likelihood, it will need additional changes when other models are investigated in the future.

LATs dominate the regular orbit composition of model E4c, probably because it is not too far from rotational symmetry around its major axis. They are less abundant than in our previous, non cuspy, model E4, although this is partly compensated by a larger abundance of SATs in the present E4c model. LATs are very scarce in the E6c model, where SATs dominate the regular orbital composition, probably because of the larger triaxiality of this model. The percentage of SATs in model E6c is larger, by a wide margin, than those of SATs and LATs taken together in our previous model E6.

The ratio of outer to inner LATs is highest in model E4c and, in fact, it is the highest of all the five models we studied; among the non cuspy models, that ratio was highest for the E4 model. It is therefore likely that such high ratios are related to the fact that those two models are close to being rotationally symmetric.

The most important resonant orbits, both in non cuspy and cuspy systems, are clearly the (x, y) fishes (3,−2,0), and they are about an order of magnitude more numerous than any other boxlets in the cuspy models.

One may wonder why we limited our search of resonances to orders 5 and 10. These choices were of course arbitrary, but it is clear that, since our frequencies are of limited precision (2×10^{-4}), if no limit were adopted it would always be possible to found some resonance of sufficiently high order. In fact, if that limit is raised to order 20, less than 1% of non-resonant boxes remain in any of our previous or present models (and none in model E6c). We think that order 5 is a reasonable limit for what one can regard as a resonant orbit, and the results that we provide for order 10 allow one to get an idea of how changing that limit might alter the results. The relationship between cuspiness and the replacing of boxes by boxlets was already known by Miralda-Escudé and Schwarzschild (1989) and our Table 8 confirms it but, besides, it also shows a correlation between triaxiality and such replacing (more triaxiality implies more boxlets at the expense of boxes). While true boxes played a

significant role among the regular orbits of our non cuspy models, their relevance is much dimished in the present cuspy ones. Although they are partially replaced by the boxlets, it is clear that the tubes are more important than boxes and boxlets taken together in cuspy systems.

We may summarize our main conclusions as follows: (1) Our models display extremely high chaoticity, with percentages of chaotic orbits up to more than 70% and they show that it is certainly possible to build self-consistent models of stellar systems that are at the same time cuspy, triaxial and highly stable. (2) Our method of regular orbit classification is very successful, with a failure rate of less than 1 in 10,000. (3) True boxes are very scarce in our cuspy models. Not only are they greatly outnumbered by the tubes, but they are also substantially scarcer than the boxlets. Even one single class of boxlets, the (x, y) fishes (3,−2,0), are almost three times more abundant than the boxes. (4) Since tubes and boxlets keep out from the systems centers, while boxes do not, the abundance of the former at the expense of the latter helps to explain the high stability of our models despite their cuspy nature.

Acknowledgements We are very grateful to Luis A. Aguilar, David Nesvorný and Daniel Pfenniger for allowing us to use their codes, to C. Kalapotharakos for the very valuable information he let us know, to Ruben E. Martínez and Héctor R. Viturro for their technical assistance and to an anonymous referee for his suggestions. This work was supported with grants from the Consejo Nacional de Investigaciones Científicas y Técnicas de la República Argentina, the Agencia Nacional de Promoción Científica y Tecnológica, the Universidad Nacional de La Plata and the Universidad Nacional de Rosario.

References

Aguilar, L.A., Merritt, D.: The structure and dynamics of galaxies formed by cold dissipationless collapse. Astrophys. J. **354**, 33–51 (1990)

Aquilano, R.O., Muzzio, J.C., Navone, H.D., Zorzi, A.F.: Orbital structure of self-consistent triaxial stellar systems. Celest. Mech. Dynam. Astron. **99**(4), 307–324 (2007)

Binney, J., Spergel, D.: Spectral stellar dynamics. Astrophys. J. **252**, 308–321 (1982)

Binney, J., Tremaine, S.: Galactic Dynamics. Princeton University Press, Princeton, NJ (2008)

Carpintero, D.D., Aguilar, L.A.: Orbit classification in arbitrary 2D and 3D potentials. MNRAS **298**(1), 1–21 (1998)

Carpintero, D.D., Wachlin, F.C.: Sensitivity of the orbital content of a model stellar system to the potential approximation used to describe it. Celest. Mech. Dynam. Astron. **96**(2), 129–136 (2006)

Contopoulos, G.: Order and Chaos in Dynamical Astronomy. Springer, Berlin (2002)

Forbes, D.A., Ponman, T.J.: On the relationship between age and dynamics in elliptical galaxies. Mon. Not. R. Astron. Soc. **309**, 623–628 (1999)

Hernquist, L., Barnes, J.: Are some N-body algorithms intrinsically less collisional than others?. Astrophys. J. **349**, 562–569 (1990)

Hernquist, L., Ostriker, J.P.: A self-consistent field method for galactic dynamics. Astrophys. J. **386**(20), 375–397 (1992)

Holley-Bockelmann, K., Mihos, J.C., Sigurdsson, S., Hernquist, L.: Models of cuspy triaxial galaxies. Astrophys. J. **549**, 862–870 (2001)

Holley-Bockelmann, K., Mihos, J.C., Sigurdsson, S., Hernquist, L., Norman, C.: The evolution of cuspy triaxial galaxies harboring central black holes. Astrophys. J. **567**, 817–827 (2002)

Jesseit, R., Naab, T., Burkert, A.: Orbital structure of collisionless merger remnants: on the origin of photometric and kinematic properties of elliptical and S0 galaxies. Mon. Not. R. Astron. Soc. **360**, 1185–1200 (2005)

Kalapotharakos, C.: The rate of secular evolution in elliptical galaxies with central masses. MNRAS **389**(4), 1709–1721 (2008)

Kalapotharakos, C., Voglis, N.: Global dynamics in self-consistent models of elliptical galaxies. Celest. Mech. Dynam. Astron. **92**(1–3), 157–188 (2005)

Kandrup, H.E., Sideris, I.V.: Chaos in cuspy triaxial galaxies with a supermassive balck hole: a simple toy model. Celest. Mech. Dynam. Astron. **82**, 61–81 (2002)

Kandrup, H.E., Siopis, C.: Chaos and chaotic phase mixing in cuspy triaxial potentials. MNRAS **345**, 727–742 (2003)

Merritt, D., Fridman, T.: Triaxial galaxies with cups. Astrophys. J. **339**, 752–762 (1996)
Miralda-Escudé, J., Schwarzschild, M.: On the orbit structure of the logarithmic potential. ApJ **409**, 563–577 (1989)
Muzzio, J.C.: Regular and chaotic orbits in a self-consistent triaxial stellar system with slow figure rotation. Celest. Mech. Dynam. Astron. **96**(2), 85–97 (2006)
Muzzio, J.C.: Regular and Chaotic Motion in Elliptical Galaxies. In: Contopoulos, G., Patsis, P. (eds.) Chaos in Astronomy, pp. 203–214. Springer, Berlin (2009)
Muzzio, J.C., Mosquera, M.E.: Spatial structure of regular and chaotic orbits in self-consistent models of galactic satellites. Celest. Mech. Dynam. Astron. **88**(4), 379–396 (2004)
Muzzio, J.C., Carpintero, D.D., Wachlin, F.C.: Spatial structure of regular and chaotic orbits in a self-consistent triaxial stellar system. Celest. Mech. Dynam. Astron. **91**(1–2), 173–190 (2005)
Napolitano, N.R., Capaccioli, M., Romanowsky, A.J., Douglas, N.G. Merrifield, M.R., Kuijken, K., Arnaboldi, M., Gerhard, O., Freeman, K.C.: Mass-to-light ratio gradients in early-type galaxy haloes. Mon. Not. R. Astron. Soc. **357**, 691–706 (2005)
Schwarzschild, M.: A numerical model for a triaxal stellar system in dynamical equilibrium. ApJ **232**, 236–247 (1979)
Schwarzschild, M.: Self-consistent models for galactic halos. ApJ **409**, 563–577 (1993)
Šidlichovský, M., Nesvorný, D.: Frequency modified Fourier transform and its application to asteroids. Celest. Mech. Dynam. Astron. **65**, 137–148 (1997)
Sparke, L.S., Sellwood, J.A.: Dissection of an N-body bar. MNRAS **225**, 653–675 (1987)
Udry, S., Pfenniger, D.: Stochasticity in elliptical galaxies. Astron. Astroph. **198**(1–2), 135–149 (1988)
Voglis, N., Kalapotharakos, C., Stavropoulos, I.: Mass components in ordered and in chaotic motion in galactic N-body models. MNRAS **337**(2), 619–630 (2002)
White, S.D.M.: Simulations of sinking satellites. Astroph. J. **274**, 53–61 (1983)